A Novel Technique for Noise Reduction in InSAR Images

ARTICLE *in* IEEE GEOSCIENCE AND REMOTE SENSING LETTERS · MAY 2007

Impact Factor: 2.1 · DOI: 10.1109/LGRS.2006.888845 · Source: IEEE Xplore

4 AUTHORS, INCLUDING:

Vidhyasaharan Sethu
University of New South Wales
30 PUBLICATIONS **164** CITATIONS
SEE PROFILE

Linlin Ge
University of New South Wales
171 PUBLICATIONS **920** CITATIONS
SEE PROFILE

A Novel Technique for Noise Reduction in InSAR Images

Dan Meng, Vidhyasaharan Sethu, Eliathamby Ambikairajah, *Member, IEEE*, and Linlin Ge, *Member, IEEE*

***Abstract*—This letter proposes a new technique for noise reduction applied to synthetic aperture radar interferometry. This technique involves a nonlinear filter that separates the interferogram into two components: one containing the smooth (low frequency) part and the other containing the detail (high frequency) part. The smooth part is obtained using a combination of a median filter and a smoothing filter. The detail component is obtained by subtracting the smooth component from the original signal. This detail component is filtered to remove noise and then added to the smooth component to generate the final output. Both simulated and real data are used to evaluate the performance of the proposed technique under different conditions. The experimental results show that the proposed technique outperforms most commonly used interferometric phase filters.**

***Index Terms*—Phase noise reduction, synthetic aperture radar interferometry (InSAR).**

I. Introduction

SYNTHETIC aperture radar (SAR) Interferometry (InSAR) is an established technique for the extraction of height information by using SAR remote sensing. It uses two high-resolution complex SAR images of the same scene to generate an interferogram. Then, the phase information contained in this interferogram is extracted to generate a digital-elevation model (DEM). As this phase information is wrapped within the interval of $[-\pi, \pi)$, it needs to be unwrapped before the estimation of height information. However, the presence of phase noise not only interferes with the phase-unwrapping process, but it also affects the quality of topographic height information obtained from the interferogram. Several techniques have been proposed in the literature to reduce interferometric phase noise. One approach, applied to the complex interferometric signal, is the multilook filter [1], which averages the values of neighboring pixels in the phase image. This technique, however, reduces noise at the expense of spatial resolution. Lee *et al.* [2] uses a local statistics filter applied to the real and the complex interferometric phase signal as well. Techniques for phase-noise reduction in the Fourier domain have also been proposed [4]. All these techniques, however, involve the loss of image detail to a certain extent.

Manuscript received January 10, 2006; revised October 31, 2006. This work was supported by the Cooperative Research Centre for Spatial Information through Project 4.2, whose activities are funded by the Australian Commonwealth's Cooperative Research Centre Programme.

D. Meng, V. Sethu, and E. Ambikairajah are with the School of Electrical Engineering and Telecommunications, The University of New South Wales, NSW 2052, Australia (e-mail: d.meng@student.unsw.edu.au; vidhyasaharan@gmail.com; ambi@ee.unsw.edu.au).

L. Ge is with the School of Surveying and Spatial Information Systems, The University of New South Wales, NSW 2052, Australia (e-mail: l.ge@unsw.edu.au).

Digital Object Identifier 10.1109/LGRS.2006.888845

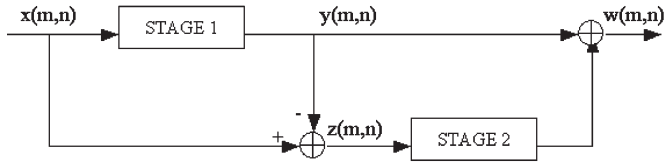

Fig. 1. Overall structure used for noise reduction involving two stages of filtering.

This letter proposes a technique that tries to minimize this loss of detail. The proposed technique involves the application of a suitable filter to remove noise, finding an estimate of the detail lost in the filtering process and reintroduction of the detail to the filtered image.

II. Two-Stage Filter Structure

The proposed technique consists of two stages of filtering, each acting on a different signal component. The first stage (smoothing filter) extracts the smooth component from the original noisy signal. The second stage operates on the detail component (difference between the original signal and the smooth component) to remove any noise present in it. In order to avoid local phase unwrapping and to overcome discontinuities of the phase signals at $-\pi$ and π, all filtering operations are performed in the complex domain.

Let the original noisy image signal be represented by $x(m, n)$, as shown in Fig. 1.

The signal $x(m, n)$ can be considered to be of the form

$$x(m,n) = S\left[s(m,n)\right] + D\left[s(m,n)\right] + \eta(m,n) \qquad (1)$$

where

$S[s(m,n)]$ smooth component of the interferogram $s(m,n)$;
$D[s(m,n)]$ detail component of the interferogram $s(m,n)$;
$\eta(m,n)$ noise component of the interferogram $s(m,n)$.

The signal $x(m, n)$ is filtered by stage 1 (smoothing filter), which preserves the smooth component $S[s(m, n)]$ while removing the noise $\eta(m, n)$ and detail $D[s(m, n)]$ components. The output of stage 1 can be given as follows:

$$y(m,n) = S\left[s(m,n)\right] + e(m,n) \qquad (2)$$

where $e(m, n)$ is the error introduced by stage 1. In an ideal case, this component would be zero.

This smooth component $y(m, n)$ is then subtracted from the original noisy signal $x(m, n)$ to obtain an estimate of the detail component that had been eliminated by stage 1. This estimate

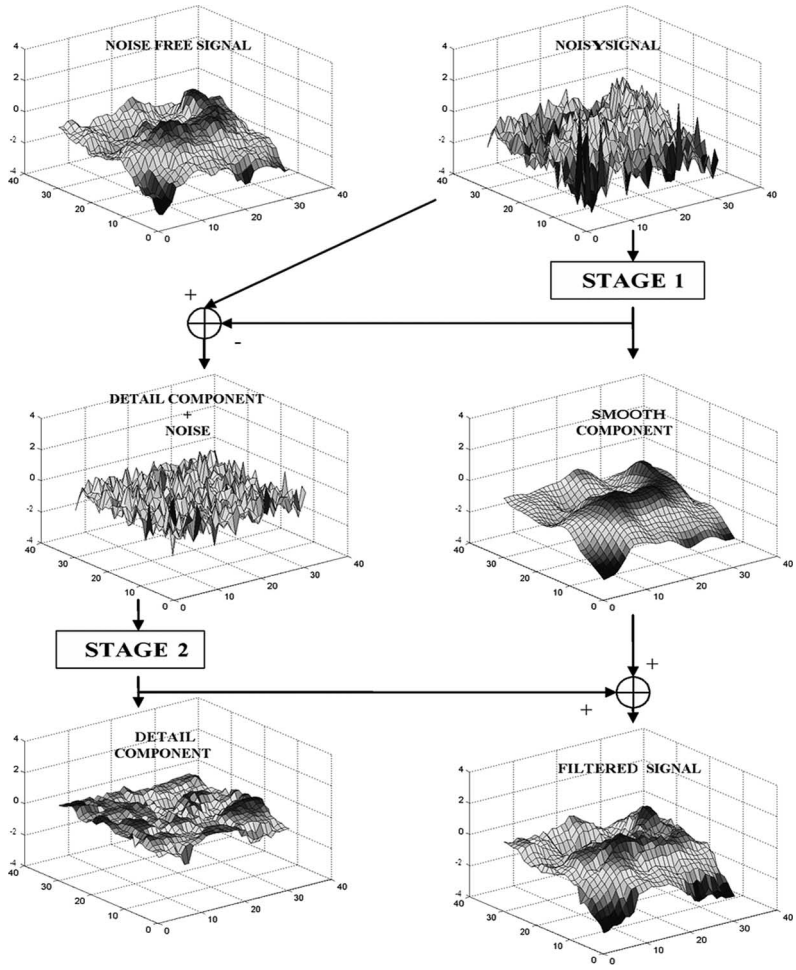

Fig. 2. Overview of the operation of the proposed structure.

$z(m,n)$, however, is corrupted by noise and can be represented as

$$z(m,n) = D\left[s(m,n)\right] - e(m,n) + \eta(m,n). \tag{3}$$

The stage 1 filter is designed such that it passes no high-frequency components; thus, the error would be composed of low-frequency components that must be reintroduced into the filtered image. Hence, it is combined with the detail component, which must also be reintroduced into the filtered image and represented as

$$\hat{D}\left[s(m,n)\right] = D\left[s(m,n)\right] - e(m,n). \tag{4}$$

The stage 2 filter (Fig. 1) operates on $z(m,n)$ to remove noise while preserving the high-frequency contents of the signal. The output is then added back to $y(m,n)$ in order to obtain a noise-free version of the input signal $x(m,n)$.

Therefore, the output of the system is the sum of the outputs of stages 1 and 2, as given in

$$w(m,n) = S\left[s(m,n)\right] + e(m,n) + \hat{D}\left[s(m,n)\right] \tag{5}$$

where $\hat{D}[s(m,n)]$ is the noise-free version of $z(m,n)$. The above nonlinear-filtering technique has been used in speech processing [5]. This is an extension of the concept of two dimensions.

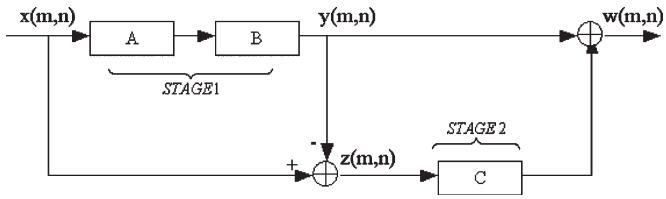

Fig. 3. Two-stage filter structure used for this letter. (a) Median filter with adaptive window. (b) Two-dimensional Vondrak filter. (c) Median filter with fixed window.

Fig. 2 illustrates the operation of the proposed two-stage filter structure (Fig. 3) using a simulated interferogram. The plots used in this figure were obtained from an interferogram simulated by the MATLAB Toolbox for InSAR [9].

It is shown that the stage 1 output is a smoothed version $y(m,n)$ of the interferogram, and although, it is devoid of noise, it has no high-frequency information, which is contained in the detail component of the signal. Reintroduction of these details by stage 2 increases the accuracy of $w(m,n)$, the estimate of the noise-free interferogram (Fig. 4).

Fig. 2 is intended to give a qualitative explanation of how the proposed structure works. Analysis of the actual performance is included in Section IV.

All the filters used in this letter operate in the complex domain. However, when signals are added or subtracted,

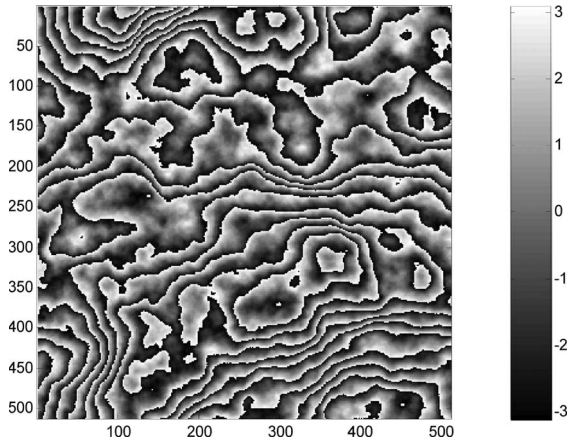

Fig. 4. Simulated interferogram without noise.

modulo-2π additions and subtractions are performed on phase data (not in the complex domain).

III. Filter Specifications

In the experimental setup, the stage 1 filter is implemented by a pivoting median filter described in [6], with its window size adapting to the local noise level, cascaded with a 2-D Vondrak filter proposed in [7]. The stage 2 filter employed is a pivoting median filter with fixed window size.

A. Stage 1 Filter—Adaptive Pivoting Median Filter

The pivoting median filters used in both stages operate on all pixels, performing nonlinear smoothing. For the stage 1 filter, however, the window within which filtering occurs is not fixed as given in [6] but is made to vary based on the coherence information corresponding to the interferogram. In order to obtain the optimum window, the average coherence per pixel is computed for all windows whose dimensions are within a specified limit, centered about the pixel on which it is operating. The window with the maximum average coherence is chosen. This gives us a median filter, where the window size and, to a certain extent, the shape adapts to the interferogram (Fig. 5).

1) Pivoting Median Filter: The following equations describe the pivoting-median filtering operation:

$$x_{\text{sum}} = \sum_{k=-(M_{\text{opt}}-1)/2}^{(M_{\text{opt}}-1)/2} \sum_{l=-(N_{\text{opt}}-1)/2}^{(N_{\text{opt}}-1)/2} x'(k,l) \tag{6}$$

$$\varphi_{\text{out}} = \underset{\substack{-(M_{\text{opt}}-1)/2 \le k \le (M_{\text{opt}}-1)/2 \\ -(N_{\text{opt}}-1)/2 \le l \le (N_{\text{opt}}-1)/2}}{\text{median}} \left\{ \arg\left(\frac{x'(k,l)}{x_{\text{sum}}} \right) \right\} + \arg(x_{\text{sum}}) \tag{7}$$

where the $x'(k,l)$ is the amplitude-normalized complex data in the window, the parameters M_{opt} and N_{opt} are the optimum window dimensions, and φ_{out} is the filter output.

2) Adaptive Window Size: For each pixel $x_{i,j}$, the average coherence inside all windows centered around $x_{i,j}$ is calculated as shown below

$$c_{\text{avg}}(m,n) = \frac{\sum_{k=i-(m-1)/2}^{i+(m-1)/2} \sum_{l=j-(n-1)/2}^{j+(n-1)/2} c_{k,l}}{m \times n} \tag{8}$$

where $c_{k,l}$ is the coherence value [8] corresponding to pixel $x_{k,l}$ and $m \times n$ is the window size with $m = 3, 5, 7, \ldots, M$ and $n = 3, 5, 7, \ldots, N$. The parameters M and N determine the maximum possible window size and can be varied. Once c_{avg} is computed for all possible windows centered on $x_{i,j}$, the window corresponding to the largest value of c_{avg} is selected and $x_{i,j}$ is replaced by $e^{j\varphi_{\text{out}}}$, where the value of φ_{out} is given by (7).

B. Stage 1 Filter—2-D Vondrak Filter

The second filter in stage 1 is a 2-D extension of the Vondrak filter described in [7]. It tries to achieve a compromise between matching the filtered curve as closely as possible to the observed data and smoothing the curve, thus preserving attributes of the original data while filtering out the noise.

For our application, we use a 2-D Vondrak filter operating with a window size of 20 $\times$ 20 pixels, with an overlap of 19 pixels. The smoothing parameters λ_1 and λ_2 are chosen based on coherence information, as described in [7], and vary for each window, thus adapting the filter parameters to the local noise statistics.

The Vondrak filtering is performed on the real and imaginary parts of the complex phase information separately, and the results are combined after filtering. Since the Vondrak filter parameters are dependent only on the coherence, for a given window, both the real and imaginary filters are identical and, thus, do not introduce any distortion. The following equations describe the Vondrak filter used in this letter:

$$\overline{\mathbf{Y}} = \left[\mathbf{I} + \frac{m}{(m-3)} \cdot \lambda_1^2 \cdot \mathbf{A}^T(m)\mathbf{A}(m) \right]^{-1} \cdot \mathbf{Y} \cdot \left[\mathbf{I} + \frac{n}{(n-3)} \cdot \lambda_2^2 \cdot \mathbf{A}^T(n)\mathbf{A}(n) \right]^{-1} \tag{9}$$

$$\lambda_1^2 = \frac{1-\overline{\rho}}{5} \quad \lambda_2^2 = \frac{1-\overline{\rho}}{500} \tag{10}$$

where $\mathbf{Y}$ is the $m \times n$ matrix representing the data within the window of size $m \times n$, $\mathbf{I}$ is the identity matrix, $\overline{\rho}$ is the average coherence inside the window, and $\mathbf{A}(p)$ is a third differentiation operator derived from a third-order Lagrange polynomial.

C. Stage 2 Filter—Fixed Pivoting Median Filter

The input to the stage 2 filter is the sum of the detail and noise components of the interferogram that was eliminated in stage 1. The stage 2 filter is designed to remove noise from this signal and obtain an estimate of the detail component. In this setup, a pivoting median filter [6] with a fixed window size of 15 $\times$ 15 pixels is used as the stage 2 filter. The choice of using a fixed window over an adaptive one is due to the fact that the coherence information used in selecting the optimum window (in the stage 1 filter) is not a good measure of the local signal-to-noise ratio of the input to this filter.

IV. Experimental Results

To analyze the performance of the proposed technique, three measures are employed.

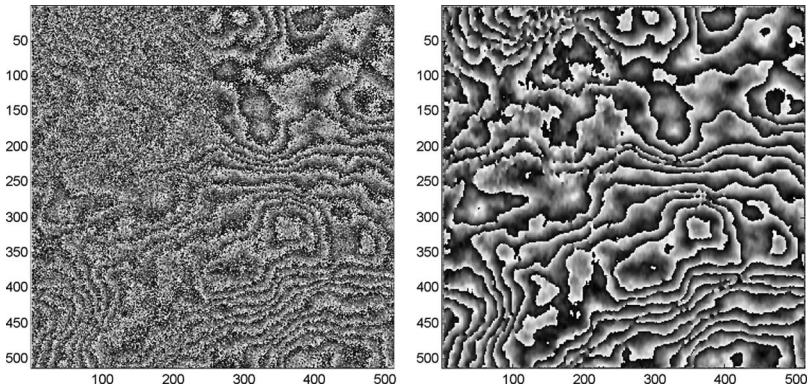

Fig. 5. Experimental data. (a) Simulated noisy interferogram with coherence values 0.2, 0.4, 0.6, and 0.8, counterclockwise from top-left quadrant. (b) Output of the proposed technique.

TABLE I
RMSE PERFORMANCE COMPARISON

Filter	RMSE for varying coherence (ρ), rad/sample				
ρ =	0.2	0.4	0.6	0.8	Avg
Boxcar (9x9)	0.73	0.52	0.58	0.42	0.57
Lee	0.83	0.53	0.41	0.29	0.55
Goldstein	1.22	0.86	0.74	0.73	0.91
Proposed Filter	0.76	0.47	0.44	0.32	0.53

The first one is an estimate of the average root mean-square error (rmse) per pixel for the filtered interferogram. A simulated interferogram (512 × 512 pixels) with perpendicular baseline (B_{perp}) of 150 m was randomly generated using the MATLAB Toolbox for InSAR [9]. Noise was modeled as an additive hypergeometrically distributed random variable according to [2], [3], and [10] and added to the simulated interferogram. The performance of the proposed technique when denoising this interferogram is compared to that of Lee, Goldstein, and Boxcar filters.

Table I compares the rmses per pixel for the outputs of different filtering techniques for varying coherence values. It is shown that the proposed technique provides the smallest average rmse. It also shows that for the area with dense fringes or steep slope, the proposed technique can smoothen the fringes without distortion.

The second and third performance measures are based on the results obtained using a real interferogram (Fig. 6) of size 1037 × 1238 pixels of an area over Appin in Australia obtained from the ERS-1/2 tandem mission. The coherence map (Fig. 7) is estimated on a 12 × 12 window for the four-look complex interferogram. The filtered image (Fig. 8) is analyzed to determine the number of residues, which is the second performance measure. Residues are local errors in the wrapped-phase values encountered during the phase-unwrapping process.

Table II compares the number of residues present in the outputs of Lee, Goldstein, and Boxcar filters with that in the output of the proposed technique. All of them operate on the same interferogram that had 414 502 residues originally.

It is worth underlining that although the total elimination of residues is the ultimate goal of filtering (which in this case would amount to no less than phase unwrapping), diminishing their number is also a very valuable result, since this drastically reduces the complexity of phase unwrapping and increases the chances of obtaining good results, as shown, for example, for a branch-cut-type algorithm [11].

It is shown that the number of residues in the interferogram filtered by the proposed technique is larger than the number of residues in the Boxcar-filtered interferogram. However,

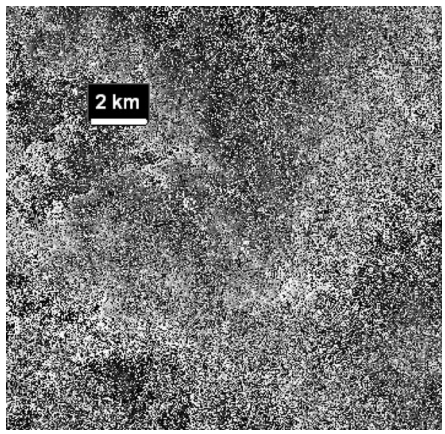

Fig. 6. Noisy interferogram obtained from the ERS-1/2 tandem pair.

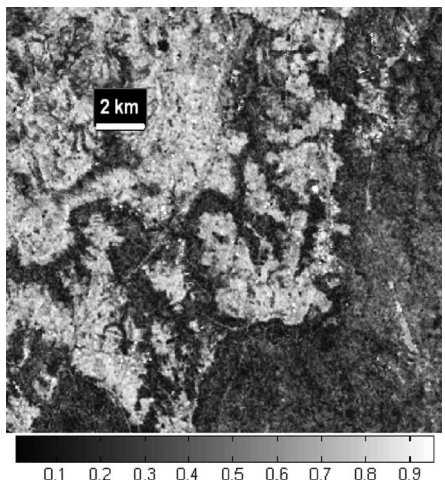

Fig. 7. Coherence map corresponding to the interferogram obtained from ERS-1/2.

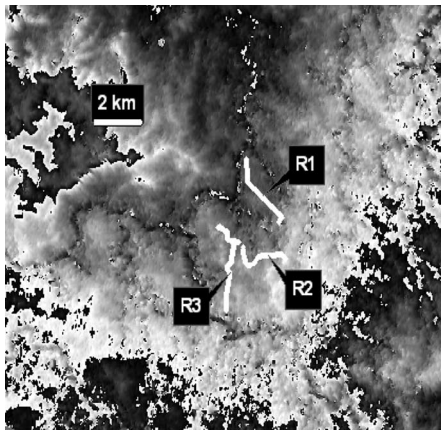

Fig. 8. Filtered interferogram using the proposed technique.

TABLE II
RESIDUE COUNT COMPARISON

Interferogram	Residues
Original (noisy)	414,502
Boxcar (13x13) [12]	2,477
Lee [3]	41,281
Goldstein [4]	121,826
Proposed Technique	6,382

TABLE III
MEAN ERROR COMPARISON (METERS)

Filter	Route 1	Route 2	Route 3
Boxcar (13x13) [12]	28.08	13.84	15.65
Lee [3]	49.59	30.51	36.64
Goldstein [4]	38.28	61.16	59.01
Proposed Technique	19.80	13.58	9.70

the number is still small and is compensated for by phase-unwrapping algorithm.

The DEM derived based on the filtered interferogram (Fig. 8) is compared to the ground truth over selected sections (routes) of the area being surveyed to give us the third performance measure. The mean error is used to measure the deviation of the estimated value from the real quantity to be estimated. In this letter, mean error is used to evaluate how much the height value in the derived DEM differs from the real topographic height. The ground-truth measurement is made every 10 m by real-time kinematic GPS with the accuracy of ± 0.04 m along the three specific routes (Fig. 8) over Appin area. The comparison of the mean errors obtained using different filters (Table III) indicates that the proposed technique gives the lowest error along all the three routes and, hence, shows its strong reliability in terms of DEM generation. The standard deviation of the errors at each point along the three routes (Table IV) is also provided to give an indication of how well the variations in the estimated data follow the variations of the actual data. The ambiguity height of the interferogram is 175.44 m.

TABLE IV
STANDARD DEVIATION OF ERROR (METERS)

Filter	Route 1	Route 2	Route 3
Boxcar (13x13) [12]	9.22	13.87	8.23
Lee [3]	11.53	18.52	9.73
Goldstein [4]	6.24	6.18	6.35
Proposed Technique	10.55	10.32	6.81

All these results show that the proposed technique performs well on both real and simulated data. In two of the three performance measures employed, it outperformed the most commonly used filters. Moreover, even though it did not give the lowest residue count, the reduction was significant so as not to overwhelm the phase-unwrapping algorithm.

V. CONCLUSION

In this letter, a new technique to reduce noise in SAR interferometric phase images has been proposed. A general two-stage structure is described into which any suitable filter can be incorporated. The image is first filtered to remove noise. Then, the removed data is analyzed, and from it, the information is extracted and reintroduced into the filtered image. The results included in this letter are generated by a system that uses a pivoting median filter with an adaptive window followed by a 2-D Vondrak filter as the smoothing filter and a pivoting median filter with a fixed window of 15×15 as the detail filter. It is shown that this technique is very effective in removing noise from SAR interferometric phase images while preserving details even when the initial noise level is high.

REFERENCES

[1] M. S. Seymour and I. G. Cumming, "Maximum likelihood estimation for SAR interferometry," in *Proc. IGARSS*, Aug. 1994, pp. 2272–2275.
[2] J. S. Lee, K. P. Papathanassiou, T. L. Ainsworth, M. H. Grunes, and A. Reigber, "A new technique for noise filtering of SAR interferometric phase images," *IEEE Trans. Geosci. Remote Sens.*, vol. 36, no. 5, pp. 1456–1465, Sep. 1998.
[3] J. S. Lee, K. W. Hoppel, S. A. Mango, and A. R. Miller, "Intensity and phase statistics of multilook polarimetric and interferometric SAR imagery," *IEEE Trans. Geosci. Remote Sens.*, vol. 32, no. 5, pp. 1017–1028, Sep. 1994.
[4] R. Goldstein and C. Werner, "Radar ice motion interferometry," in *Proc. 3rd ERS Symp. Space Service Environ.*, 1997, pp. 969–972.
[5] L. R. Rabiner and R. W. Schafer, *Digital Processing of Speech Signals*. Englewood Cliffs, NJ: Prentice-Hall, 1978.
[6] T. Zhi, L. Jingwen, and Z. Yinging, "Analysis on noise reduction method for interferometric SAR image," in *Proc. IGARSS*, 2004, vol. 6, pp. 4243–4346.
[7] X. Ding, Z. Li, D. Zheng, C. Huang, and W. Zou, "SAR interferogram filtering with 2-D Vondrak filter," in *Proc. IGARSS*, 2005, vol. 7, pp. 4825–4828.
[8] R. Bamler and P. Hartl, "Synthetic aperture radar interferometry," *Inv. Probl.*, vol. 14, no. 4, pp. R1–R54, 1998.
[9] B. Kampes and S. Usai, "Doris: The Delft object-oriented radar interferometric software," in *Proc. ITC 2nd ORS Symp.*, Aug. 1999, 4 pp. CD-ROM.
[10] C. Lopez-Martinez and X. Fabregas, "Modeling and reduction of SAR interferometric phase noise in the wavelet domain," *IEEE Trans. Geosci. Remote Sens.*, vol. 40, no. 12, pp. 2553–2566, Dec. 2002.
[11] G. Ferraiulo and G. Poggi, "A Bayesian filtering technique for SAR interferometric phase fields," *IEEE Trans. Image Process.*, vol. 13, no. 10, pp. 1368–1378, Oct. 2004.
[12] R. C. Gonzalez and R. E. Woods, *Digital Image Processing*, 2nd ed. Englewood Cliffs, NJ: Prentice-Hall, 2003.